Received: 12 May 2020 | Revised: 25 August 2020 | Accepted: 28 August 2020

DOI: 10.1002/edn3.137

SPECIAL ISSUE ORIGINAL ARTICLE

Environmental DNA
Open Access
Dedicated to the study and use of environmental DNA for basic and applied sciences

WILEY

How to design optimal eDNA sampling strategies for biomonitoring in river networks

Luca Carraro[1,2] | **Julian B. Stauffer**[1,2,3] | **Florian Altermatt**[1,2,4]

[1]Department of Evolutionary Biology and Environmental Studies, University of Zurich, Zürich, Switzerland

[2]Department of Aquatic Ecology, Swiss Federal Institute of Aquatic Science and Technology (Eawag), Dübendorf, Switzerland

[3]Research Division 3: Marine Ecology, GEOMAR Helmholtz Centre for Ocean Research, Kiel, Germany

[4]University Research Priority Programme (URPP) on Global Change and Biodiversity, University of Zurich, Zürich, Switzerland

Correspondence

Luca Carraro, Department of Evolutionary Biology and Environmental Studies, University of Zurich, Zürich, Switzerland.Email: luca.carraro@eawag.ch

Luca Carraro, Department of Evolutionary Biology and Environmental Studies, University of Zurich, Zürich, Switzerland.

Funding information

Swiss National Science Foundation, Grant/Award Number: PP00P3_179089 and 31003A_173074; University of Zurich

Abstract

The current biodiversity crisis calls for appropriate methods for assessing biodiversity. In this respect, environmental DNA (eDNA) holds great promise, especially for aquatic ecosystems. While initial eDNA studies assessed biodiversity at single sites, technology now allows analyzing samples from many points simultaneously. However, the selection of these sites has been mostly motivated on an ad-hoc basis. To this end, hydrology-based models might offer a unique guidance on where to sample eDNA to most effectively reconstruct spatial patterns of biodiversity. Here, we performed computer simulations to identify best-practice criteria for the choice of positioning of eDNA sampling sites in river networks. To do so, we combined a hydrology-based eDNA transport model with a virtual river network reproducing the scaling features of real rivers. In particular, we conducted simulations investigating scenarios of different number and location of eDNA sampling sites in a riverine network, different spatial taxon distributions, and different eDNA measurement errors. We found that, due to hydrological controls, non-uniform patterns of eDNA concentration arise even if the taxon distribution is uniform and decay is neglected. Best practices for sampling site selection depend on the taxon's spatial distribution: when taxa are concentrated in some hotspots and only few sampling sites can be placed, it is better to preferentially locate them in the downstream part of the catchment; when taxa are more evenly distributed, and/or many sites can be placed, these should be preferentially located upstream. We also found that uncertainties in eDNA concentration estimates do not necessarily hamper model predictions. Knowledge of eDNA decay rates improves model predictions, highlighting the need for empirical estimates of these rates under relevant environmental conditions. Our simulations help define strategies for designing eDNA sampling campaigns in river networks and can guide the sampling effort of field ecologists and environmental authorities.

KEYWORDS

eDITH, environmental DNA, freshwater biodiversity, Optimal Channel Network, riverine network, sampling design

1 | INTRODUCTION

The recently released report by the Intergovernmental Science-Policy Platform on Biodiversity and Ecosystem Services (IPBES) shows that global biodiversity is declining in an unprecedented way, and effective societal and policy responses are needed now more than ever (IPBES, 2019). While all ecosystems are affected, showing both strong declines in biodiversity and associated ecosystem functions, freshwater ecosystems (and riverine ecosystems in particular) are among the most concerned. Changes in land use, climate, damming and hydropower, and chemical pollution heavily impair riverine ecosystems (Darwall et al., 2018; Reid et al., 2019; Vörösmarty et al., 2010), such that their status is a matter of primary societal and political concern (Dudgeon, 2019). These changes call for a rapid understanding and documentation of the state but also change of biodiversity. Adequate strategies for freshwater biodiversity preservation must thus adopt efficient monitoring tools, and comprise strategies that acknowledge the characteristic spatial structure of river networks and their biodiversity (Altermatt, 2013). In this context, the use of environmental DNA (eDNA) constituted a major breakthrough of the last decade (Beng & Corlett, 2020; Bohmann et al., 2014; Ficetola, Miaud, Pompanon, & Taberlet, 2008; Kelly et al., 2014; Thomsen & Willerslev, 2015). The eDNA technique consists in the detection of organisms based on their DNA extracted from environmental samples (e.g., from soil or water) (Taberlet, Coissac, Hajibabaei, & Riesenberg, 2012) and can cover organisms ranging from bacteria to eukaryotes. Compared to traditional species sampling methods, eDNA has the advantage of being minimally invasive and fast, yet able to detect multiple species thanks to metabarcoding (Deiner et al., 2017; Pawlowski et al., 2018), including rare and elusive species (Jerde, Mahon, Chadderton, & Lodge, 2011; Mächler, Deiner, Steinmann, & Altermatt, 2014). This gives the potential for biodiversity assessments at high spatial and temporal resolutions (Altermatt et al., 2020; Bohmann et al., 2014; Pawlowski et al., 2018).

A key feature of such a spatially and temporally highly resolved biodiversity assessment is maximizing the quantity and quality of the data gathered with as little effort as possible. While initial studies on biodiversity assessments in riverine ecosystems sampled at one or few locations within a single watershed, without the goal of a catchment-level perspective (e.g., Mächler et al., 2014; Thomsen et al., 2012), more recent works with a biodiversity focus aimed at resolving diversity across the whole catchment (Carraro, Mächler, Wüthrich, & Altermatt, 2020; Deiner, Fronhofer, Mächler, Walser, & Altermatt, 2016; Mächler et al., 2019; Sales et al., 2020). This immediately brings up the question of where to sample, and how many samples to take, to effectively assess biodiversity across a catchment. The costs of sampling and processing of eDNA may scale much less than linearly, both in terms of financial and time costs (Sengupta et al., 2019); however, to maximize the efficiency of eDNA, optimizing sampling strategies is paramount. Guidelines on where to best take eDNA samples in river networks are thus needed, and these guidelines must consider the origin, transport, and decay of eDNA along the waterway.

Research on molecular and bioinformatic aspects of eDNA analyses has massively expanded within the last few years (Alberdi, Aizpurua, Gilbert, & Bohmann, 2017; Beng & Corlett, 2020; Calderón-Sanou, Münkemüller, Boyer, Zinger, & Thuiller, 2019; Deiner et al., 2017; Ficetola, Taberlet, & Coissac, 2016; Garlapati, Charankumar, Ramu, Madeswaran, & Ramana Murthy, 2019; Leray, Knowlton, Ho, Nguyen, & Machida, 2019). Much less focus, however, has been attributed to the "ecology of eDNA," namely "its origin, state, transport, and fate within the environment" (Barnes & Turner, 2015), and how these factors influence its detection (Barnes & Turner, 2015; Harrison, Sunday, & Rogers, 2019). Indeed, in riverine environments, hydrological transport of material containing genetic information makes eDNA a carrier of information on biodiversity of the upstream catchment (Deiner et al., 2016). While this fact underlines the crucial role of eDNA as a tool to monitor biodiversity at large scales, it also gives rise to further challenges with respect to the reconstruction of spatial patterns of biodiversity. Essentially, the eDNA sampled at a river's cross-section results from the aggregation of the dynamics of particle transport from a number of upstream sources (i.e., the locations of the target species) along a dendritic river network toward the sampling site. Importantly, eDNA advection is subject to decay processes typically dependent on several abiotic and biotic factors, as well as on hydrological conditions (Barnes et al., 2014; Shogren et al., 2017; Strickler, Fremier, & Goldberg, 2015), resulting in downstream traveling distances ranging from meters to tens or hundreds of kilometers (Deiner & Altermatt, 2014; Jane et al., 2015; Pont et al., 2018; Sansom & Sassoubre, 2017; Shogren et al., 2017). Thus, it is clear that comprehensive eDNA studies in riverine environments cannot ignore hydrological and geomorphological concepts. Research at the boundary between hydrology and molecular ecology is needed, as the sole focus on the molecular aspects of eDNA analyses would lead to an incomplete application of the method and undermine its power as a biomonitoring tool.

Recently, physically based models with different degrees of complexity have been developed in order to assess dynamics of transport and decay of eDNA in water. Sassoubre, Yamahara, Gardner, Block, and Boehm (2016) applied a simple mass-balance model to a tank experiment; Shogren et al. (2016) studied eDNA transport in a column experiment; Shogren et al. (2017) used a simple transport model in a flume experiment; Nukazawa, Hamasuna, and Suzuki (2018) and Sansom and Sassoubre (2017) formulated 1D advection models in river stretches; Andruszkiewicz et al. (2019) and Fukaya et al. (2020) applied 3D advection–diffusion equations to study eDNA transport in marine bays. Carraro et al. (2017) and Carraro, Hartikainen, Jokela, Bertuzzo, and Rinaldo (2018) coupled a first-order formulation of eDNA decay with well-established knowledge on the geomorphology and hydraulic properties of river networks (Leopold & Maddock, 1953; Rodriguez-Iturbe & Rinaldo, 2001) to infer the upstream distribution of target species based on eDNA data sampled at multiple locations across the river network. The ability of such types of models to accurately predict

spatial patterns of biodiversity substantially relies on the accuracy of the eDNA measurements. However, literature on an optimal layout of eDNA sampling strategies is rather poor: Dickie et al. (2018) reviewed practices of sampling protocols in terrestrial and freshwater eDNA studies, but did not specifically address the issue of positioning eDNA sampling sites across a river network; Bylemans et al. (2018) studied the effect of sampling intensity and replication at fixed sampling sites on the estimation of fish biodiversity in a river, and found that a larger number of replicates at downstream sites is needed to fully assess biodiversity; Wood, Erdman, York, Trial, and Kinnison (2020) observed that, due to transverse hydrodynamic dispersion, detection rates are maximized if eDNA is collected at some distance downstream of a known source, otherwise the dispersion plume of eDNA would likely be missed.

No studies to date, however, have investigated the optimal positioning of sampling sites across whole catchments, although such information would be highly relevant to the effectiveness of eDNA sampling campaigns in rivers. Here, we fill this gap by making use of computer simulations in order to assess different scenarios of eDNA release, transport, and detection. We test these scenarios based on the application of the hydrology-based eDNA transport model of Carraro, Hartikainen, et al. (2018) using synthetic analogues of river networks (so-called Optimal Channel Networks, see Carraro, Bertuzzo, et al. (2020) and Rinaldo, Rigon, Banavar, Maritan, and Rodriguez-Iturbe (2014)). This allows testing realistic spatial scenarios in a generic setting that is not constrained to the particular shape of a real river network. In the studied scenarios, we explored varying numbers and locations of the sampling sites, spatial distributions of the target species as a proxy of eDNA release, and assumptions on decay rate and eDNA measurement errors. Together, this allowed the identification of generalizable rules of optimal eDNA sampling strategies in rivers.

2 | MATERIALS AND METHODS

This section is structured as follows: first, we introduce the tools needed for the subsequent computer simulations, namely an eDNA transport model and a virtual river network; second, we show how such tools are used to assess patterns of eDNA concentration across a river produced by particular spatial distributions of taxon density and decay rate values; third, we describe the strategy and details of the computer simulations aimed at assessing optimal eDNA sampling strategies. Note that, as this section substantially relies on mathematical formulations, we introduce every subsection with a brief description in which the relevant information is outlined, then followed by the more technical details. All mathematical symbols used in the following, as well as the respective dimensions, are listed in Table S1.

2.1 | The eDITH model

To simulate transport of eDNA in the water across a river network, we utilize the approach of Carraro, Hartikainen, et al. (2018), subsequently referred to as eDITH (*e*DNA *I*ntegrating *T*ransport and *H*ydrology). This approach exploits knowledge on hydrology and geomorphology of river networks to transform a map of eDNA production p across a catchment into a map of eDNA concentration C in stream water. As a first approximation, p can fairly be assumed to be proportional to relative taxon density (see Carraro, Hartikainen, et al., 2018, for a discussion on caveats of this assumption), which enables considering the eDITH model as a function that relates a spatial distribution of taxon density to a spatial distribution of eDNA concentration. Note that we do not make specific assumptions on the molecular state of the DNA extracted from the environment; we only assume that organisms can be detected based on their DNA in environmental samples, and that this DNA signal is subject to generic processes describing production, transport, and decay.

Notably, the eDITH model can be used in two different ways. First, assuming that the spatial distribution of a taxon is known, it allows transforming such distribution into the corresponding pattern of eDNA concentration. Second, eDITH can be used in an inverse modeling approach, where eDNA concentrations at some locations within the river network are measured, and the model is used to infer what is the pattern of p that is most likely to have generated such values of eDNA concentration. In the following application, both uses of the eDITH model will be employed.

Note that all parameters involved in the relationship between C and p (except the decay rate) relate to the morphology of the river network and can thus be assessed with sufficient precision with a combination of GIS-based river network extraction, field observations, and power–law scaling relationships for the hydraulic variables of interest (Leopold & Maddock, 1953; O'Callaghan & Mark, 1984; Rodriguez-Iturbe & Rinaldo, 2001). The value of the eDNA decay rate can be directly inferred from model calibration; alternatively, specific information on eDNA decay dynamics (if available) could be used to define such value (or, at a minimum, a range thereof), thus likely improving the model's prediction skill.

Technical details of the eDITH model are hereafter provided. Let us consider a river network discretized into N nodes. The partitioning of the river network into nodes must be operated such that, within each node, both hydrological conditions and taxon density can reasonably be assumed as homogeneous. For a given taxon, the eDNA concentration C_j at node j can be expressed as:

$$C_j = \frac{1}{Q_j} \sum_{i \in \gamma(j)} A_{s,i} \exp\left(-\frac{L_{ij}}{v_{ij}\tau}\right) p_i \quad (1)$$

where Q_j is a characteristic value of water discharge at node j; $\gamma(j)$ identifies the set of nodes upstream of j; $A_{s,i}$ is the source area (i.e. the habitat extent) of node i; p_i is the eDNA production rate at node i; $\exp[-L_{ij}/(v_{ij}\tau)]$ is a first-order exponential decay factor, in which L_{ij} is the length of the path between i and j, v_{ij} the average water velocity along this path, and τ a characteristic decay time for the taxon's eDNA in running water. The decay time τ is a value indicative of the timescale of the decay process (expressed as the inverse of a decay rate), which accounts for all sources of eDNA depletion, from degradation to

gravity-induced deposition; hence, τ is not the time at which all eDNA is degraded; therefore, its definition is independent of the starting concentration. For a water-dwelling taxon (the case that we investigate in this application), $A_{S,i}$ can be seen as the water surface area at node i: $A_{S,i} = L_i w_i$, where L_i and w_i are the length and width of the river stretch corresponding to node i, respectively.

2.2 | Optimal Channel Networks

The virtual river network used in the following simulations is an Optimal Channel Network (OCN) built via the R-package *OCNet* (Carraro, Altermatt, et al., 2020; Carraro, Bertuzzo, et al., 2020). OCNs are idealized constructs that reproduce the topological and scaling features of real river networks and are therefore suitable for simulation studies on various ecological and ecohydrological issues (Rinaldo et al., 2014; Rodriguez-Iturbe et al., 1992). In this application, we analyze the outputs of the eDITH model on an OCN that represents a catchment covering an area of 400 km^2 (Figure 1).

The OCN is built on a square lattice whose side is made up of 400 pixels, each of which is assumed to represent a 50-m by 50-m cell. A threshold area of 461 pixels ($A_T = 461 \cdot 0.05^2 = 1.15\,\text{km}^2$) is used to distinguish the fraction of lattice pixels that effectively constitute the river network. At this so-called RN (river network) aggregation level, the network is constituted by 4,468 nodes (each corresponding to a 50-m pixel with drainage area $\geq A_T$; see Carraro, Bertuzzo, et al. (2020) for details on aggregation levels of an OCN). Subsequently, such network is further coarsened into the AG (aggregated) level, where nodes represent sources and confluences of the network at the RN level, while edges follow the drainage directions previously identified. Additional nodes are added in order to split the edges into portions not longer than 2.5 km (option *maxReachLength* in function *aggregate_OCN* of *OCNet*). Such maximum length value is arbitrarily imposed in order to partition the OCN into reaches of limited size, where abiotic (water discharge and velocity) and biotic (taxon density) variables could, as a first approximation, be considered homogeneous (although we acknowledge that the spatial extent of a niche may be taxon dependent). The resulting number of nodes at the AG level is 201. Note that, since all nodes except the outlet node are associated to an edge directed downstream, the river network at the AG level is essentially partitioned into 200 segments, while the outlet node is immaterial. The choice of the value of A_T is purposely operated to obtain a partitioning of the river network into 200 segments. According to a well-established approach in hydrology (Leopold & Maddock, 1953; Rodriguez-Iturbe & Rinaldo, 2001), water discharge Q, river width w, and water velocity v across the whole river network are calculated via power-law functions of drainage area A:

$$Q_i = Q_o \left(\frac{A_i}{A_o}\right); \quad w_i = w_o \left(\frac{A_i}{A_o}\right)^{0.5}; \quad v_i = v_o \left(\frac{A_i}{A_o}\right)^{0.1}, \tag{2}$$

where subscript o identifies the outlet node. The values specified at the outlet node are Q_o = 10 m^3/s, w_o = 10 m, v_o = 1 ms^{-1}, A_o = 400 km^2. The chosen value of Q_o implies a specific discharge of $Q_o/A_o = 0.025$ m^{3}s^{-1}km^{-2}, which resembles typical values for prealpine catchments (Carraro, Mari, Gatto, Rinaldo, & Bertuzzo, 2018; Schädler & Weingartner, 1992).

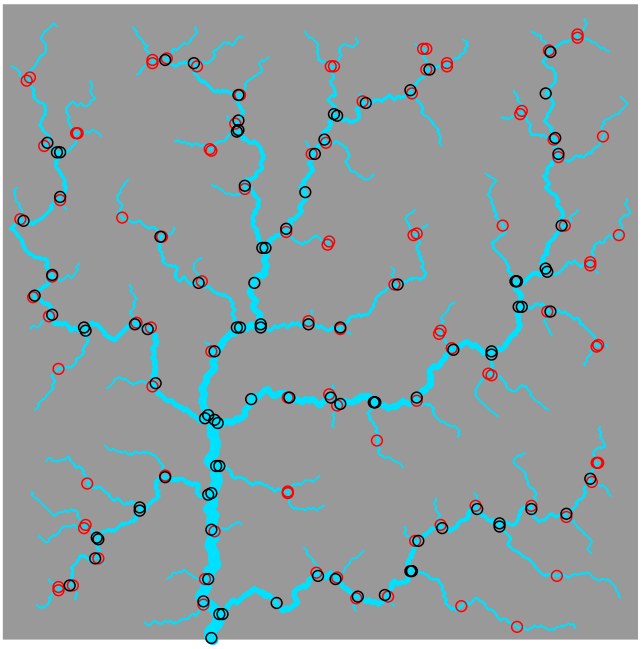

FIGURE 1 Representation of the optimal channel network used in this study, spanning a square of side 20 km. The aggregation of the OCN at the AG level (see Carraro, Bertuzzo, et al., 2020) identifies 200 nodes, which are here displayed at the downstream end of the corresponding river reaches. Red indicates nodes whose drainage area is lower than the median drainage area across the 200 nodes (referred to in the text as upstream nodes); black identifies nodes with drainage area higher than the median (downstream nodes)

2.3 | Analysis of eDNA concentration patterns across a river network

A first set of simulations aims at qualitatively assessing patterns of eDNA concentrations across the OCN produced by some peculiar distributions of taxon density (expressed as eDNA production rates p) and different values of the decay time τ (fast decay: τ = 1 hr; intermediate decay: τ = 4 hr; no decay: $\tau \to \infty$). Decay times of eDNA are known to vary widely as a function of abiotic conditions, such as temperature, pH, and acidity, with the order of magnitude being equal to some hours (see e.g., Eichmiller, Best, & Sorensen, 2016; Seymour et al., 2018; Tsuji, Ushio, Sakurai, Minamoto, & Yamanaka, 2017). Note that most studies assess decay rates in laboratory conditions, while estimates obtained from field data often lead to lower values of τ because of deposition phenomena and environmental factors such as presence of riverbed biofilm (Nukazawa et al., 2018; Shogren et al., 2018). Our choice of τ values thereby enables us to explore the widest possible (and meaningful) range for this parameter.

We here compare the eDNA concentration patterns resulting from the two most distinct distributions of taxon density: On the one hand, a uniform distribution, in which the density (i.e., biomass per unit habitat area) of a taxon is evenly distributed across the whole river network, thereby representative of a generalist species; on the other hand, a distribution related to a unique point source, in which the taxon is only present at the node that is farthest from the outlet. The latter represents a rare species, specialized to headwater streams. Indeed, any other spatial pattern of taxon density can be seen as a combination of these two distributions. The uniform distribution is obtained by setting $p_i = 1$ mol/(m^2·s) $\forall\, i = 1, \ldots, N$. The unit for p expresses the fact that production rates are amounts of substance (i.e., DNA) per unit habitat area and unit of time (Carraro, Hartikainen, et al., 2018). However, units are immaterial in our application, thus we will hereafter refer to a normalized production rate $\overline{p}_i$, which is equal to 1 $\forall\, i = 1, \ldots, N$ in the uniform distribution case. To enable comparison with the uniform case, the point source distribution is defined by:

$$\overline{p}_k = \frac{\sum_{i=1}^{N} A_{S,i}}{A_{S,k}}; \quad \overline{p}_j = 0 \quad \forall\, j \neq k, \tag{3}$$

where k identifies the node that is farthest from the outlet. Equation (3) assumes that all the amount of eDNA (per time unit) produced across the river network in the uniform case is now located in node k. Note that we enforce equal total taxon abundance across all types of taxon distributions in order to be able to effectively compare the eDNA concentration patterns resulting from these maps. However, taxon distribution patterns found in nature may indeed depart from this assumption (e.g., in the case of a rare taxon, found only in few locations with low density therein).

In an analogous way, the eDNA concentrations resulting from the application of the eDITH model to these spatial distributions of $\overline{p}$ are also normalized in order to facilitate comparison. Normalized concentrations $\overline{C}_j$ are calculated as:

$$\overline{C}_j = \frac{C_j Q_o}{\sum_{i=1}^{N} A_{S,i}}, \tag{4}$$

where $\sum_{i=1}^{N} A_{S,i}/Q_o$ is the concentration that would be measured at the outlet under the hypothesis of no eDNA decay ($\tau \to \infty$ in Equation (1)).

In this first exercise, we make use of the refined OCN aggregated at the RN level (N = 4,468).

2.4 | Assessing the effect of sampling strategy

2.4.1 | Overview

In a second phase, we combine the tools hitherto presented in order to assess the effectiveness of different eDNA sampling strategies across a river network. In particular, we adopt the "virtual ecologist" approach proposed by Zurell et al. (2010), whereby we couple simulated data and an observation model to mimic the distribution of a species, and subsequently infer properties of the observation model. An overview of the sequence of performed operations is shown in Figure 2. The first step consists in building maps of (normalized) taxon density $\overline{p}^{\text{sim}}$ that potentially resemble realistic density maps. Second, we run the eDITH model (Equation (1) and (4)) on these maps and yield patterns of (normalized) eDNA concentration $\overline{C}^{\text{sim}}$. Third, we formulate different sampling strategies in terms of intensity (i.e., number of sampling sites) and positioning (i.e., preference for upstream/downstream location of sites); we then randomly sample sites (i.e., nodes of the network) according to a given strategy, and assume to "observe" the concentration $\overline{C}^{\text{obs}}$ therein (i.e., equal to $\overline{C}^{\text{sim}}$ as calculated in step 2, possibly with a measurement error). Fourth, we fit the eDITH model on these observed concentrations, and find a predicted pattern of eDNA production $\overline{p}^{\text{mod}}$ that best reproduces the observed concentrations. Fifth, we compare the resulting maps $\overline{p}^{\text{mod}}$ with the original solution $\overline{p}^{\text{sim}}$ generated in step 1, and assess the prediction skill of the model. All steps are repeated a sufficient number of times to account for the various sources of stochasticity. We adopt a full factorial design, whose factors are listed in Table 1. The total number of simulations performed is 4,500. Details on the factors and levels are hereafter provided. In order to reduce the dimensionality of the problem, this analysis is performed on the OCN aggregated at the AG level (N = 200).

2.4.2 | Generation of maps of taxon density

The taxon distribution maps previously introduced (i.e., uniform density versus point source located at the farthest headwater) represent idealized constructs that were introduced for illustrative purposes, although they might be only partially representative of a real taxon distribution. Here instead, we generate more realistic taxon density maps (see e.g., Alther & Altermatt, 2018; Besemer et al., 2013; Kaelin & Altermatt, 2016; Little, Fronhofer, & Altermatt, 2020) characterized by a certain number of hotspots across the network, where the taxon is most abundantly located. In particular, we focus on two types of distributions: a first type, mimicking the distribution of a taxon with scattered distribution (termed S), with few hotspots where the taxon density is high; a second type (E), representing the distribution of a more evenly distributed taxon, with many hotspots in which the taxon density is lower as compared to the previous case.

Taxon density maps are generated by randomly sampling (without replacement) N_H hotspot nodes among the N nodes constituting the OCN. On these hotspot nodes, a temporary value of density $\overline{p}'$ equal to x is attributed, while all other network nodes are initially attributed $\overline{p}' = 0$. Next, all nodes immediately downstream or upstream of the hotspot nodes are attributed an additional $x/2$ density (summed to 0 if that node had not been selected, or to x or $x/2$ otherwise). The so-obtained temporary densities $\overline{p}'$ are transformed into a normalized density map via:

$$\overline{p}_j^{\text{sim}} = \frac{\overline{p}_j' \sum_{i=1}^{N} A_{S,i}}{A_{S,j} \sum_{i=1}^{N} \overline{p}_j'} \quad \forall\, j = 1, \ldots, N, \tag{5}$$

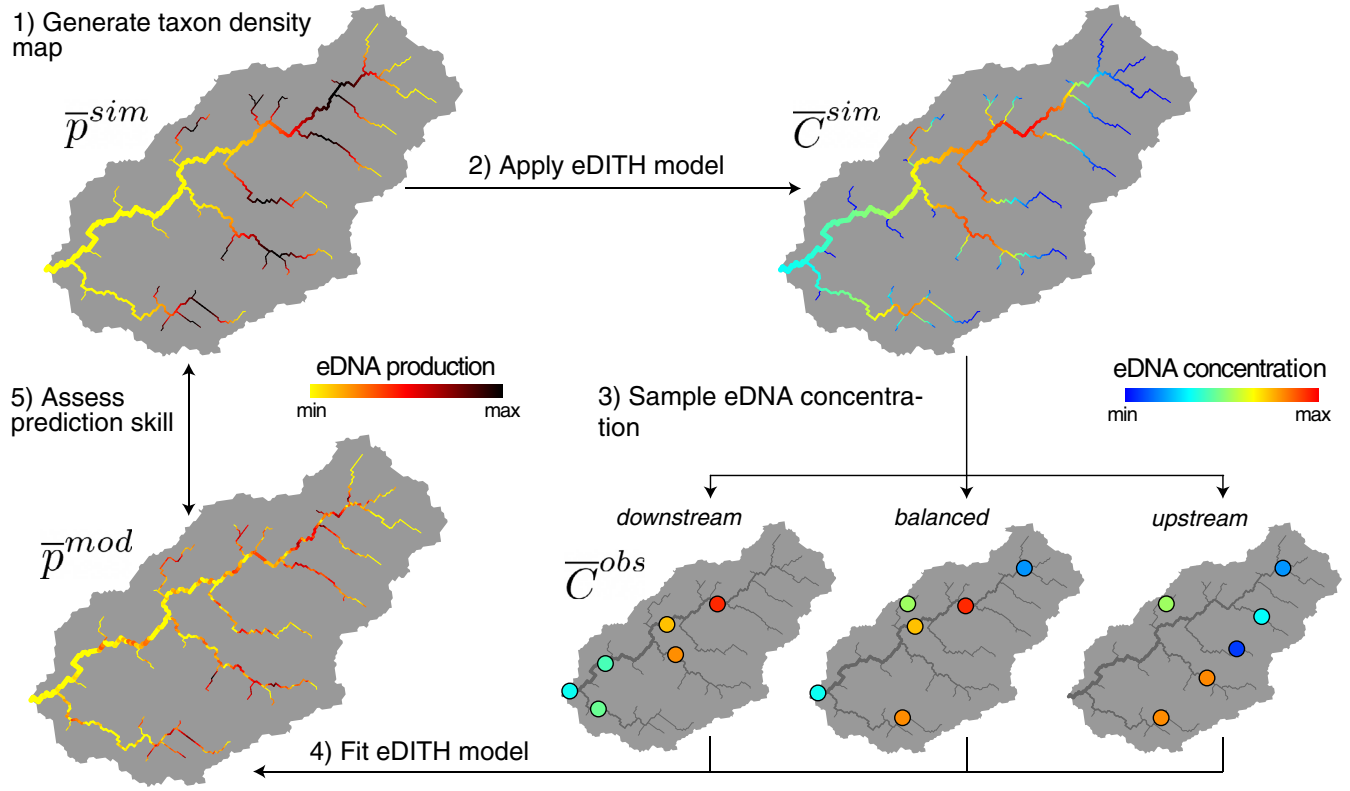

FIGURE 2 Overview of the computer simulations. In step 1, taxon density maps $\overline{p}^{sim}$ are generated; the example shows a taxon that is abundant only within a narrow elevational range. In step 2, by applying the eDITH model with $\tau = 4$ hr, corresponding patterns of eDNA concentration $\overline{C}^{sim}$ are evaluated. In step 3, following a given sampling strategy (number and location of sampling sites; here, for the same number of sampling sites, three strategies, characterized by differential preference for downstream or upstream reaches, are shown), $\overline{C}^{obs}$ are observed at the sampling locations. In step 4, the eDITH model is fitted on$\overline{C}^{obs}$, yielding to a modeled taxon distribution $\overline{p}^{mod}$. The latter is compared with the original $\overline{p}^{sim}$ in step 5 to assess the prediction skill of the sampling strategy

which satisfies the normalization constraint $\sum_{i=1}^{N} \overline{p}_i^{sim} A_{S,i} = \sum_{i=1}^{N} A_{S,i}$ (as in Equation (3)). For the scattered (S) distribution type, we set $N_H = 5$, while for type E, we set $N_H = 50$. Note that these are arbitrary values, which nevertheless enable building realistic and distinguishable patterns of taxon density (Alther & Altermatt, 2018; Besemer et al., 2013; Kaelin & Altermatt, 2016; Little et al., 2020). For each of these distribution types, five different maps are built (see Figure 3).

In step 2 of the computer simulations, we generate (via eDITH) patterns of $\overline{C}^{sim}$based on the previously derived taxon distribution maps $\overline{p}^{sim}$and by fixing τ = 4 hr. Note that we assume that sampling sites be located at the downstream end of the river reach to which they are associated. As a result, if i is a headwater node (i.e.,$\gamma(i) = \{i\}$), the normalized concentration at this site is given by $\overline{C}_i^{sim} = L_i w_i \exp\left[-L_i/(v_i\tau)\right] \overline{p}_i^{sim}/Q_i$. Maps of simulated eDNA concentration patterns are shown in Figure 3.

2.4.3 | Sampling strategies

Three different levels of sampling intensity (i.e., number of sampled nodes, where $\overline{C}^{obs}$ is observed) are adopted: 10%, 25% and 50% of the available network nodes, corresponding to 20, 50 and 100 sampling sites, respectively. For a given level of sampling intensity, five different schemes for sites' location are investigated. These are defined with the acronyms U0, U20, U50, U80, U100, where the number identifies the percentage of sites that are positioned in the upstream half of the catchment (i.e., among the network nodes whose drainage area A is lower than the median of A; see Figure 1), while the remaining fraction is sampled among the downstream network nodes. For example, the sampling strategy 10%-U20 consists of 20 sampling nodes, where one fifth of them (4 nodes) are picked from the upstream half of the catchment, and the remaining 16 are chosen within the downstream half. For each sampling strategy, 10 different sets (termed realizations) of sampling nodes are generated, resulting in a total of 150 sets of sites. Note that the 10 realizations corresponding to strategies 50%-U0 and 50%-U100 actually constitute repetitions of the same set of sampling nodes (the 100 nodes depicted in Figure 1 in black and red, respectively). The different sampling designs were characterized in terms of nestedness (i.e., fraction of sites connected by flow) and mean pairwise along-stream distance (see Appendix S1 and Figures S1 and S2).

2.4.4 | Model variants

We make different assumptions with respect to the quality of information available on eDNA concentration values and the decay dynamics thereof. In particular, we formulate different model variants, in which we distinguish cases where the eDNA decay rate is known or unknown, and cases where eDNA concentrations at the sampling sites are observed with or without measurement errors (including non-detections).

TABLE 1 Factors and levels of the full factorial design used in the computer simulations

Scope	Factor	Number of levels	Level names
Taxon distribution	Type	2	S, E
	Realization	5	1, 2, 3, 4, 5
Sampling strategy	Intensity	3	10%, 25%, 50%
	Positioning	5	U0, U20, U50, U80, U100
	Realization	10	–
Model variant	-	3	TF, TU, ME

Note: Types of taxon distribution: S ("scattered"), E ("even"); for each of these types, 5 different realizations are generated (see Figure 3). Intensity is expressed as percentage of nodes of the river network that are sampled; positioning represents the percentage of such sites that are located in the upstream half of the catchment (e.g., U20: 20% of the sites are located upstream); for each combination of intensity and positioning, 10 different sampling designs are generated (see one example in Figures S5 and S6). Model variants are TF ("tau fixed"), TU ("tau unknown"), ME ("measurement error").

In a first model variant (termed TF, "tau fixed"), we assume that, in step 4 (model fitting), τ is known to be equal to 4 hr, and therefore, the only unknown parameters are the $\overline{p}^{\mathrm{mod}}$values across the 200 network nodes. Moreover, no measurement error is assumed, hence $\overline{C}^{\mathrm{obs}} = \overline{C}^{\mathrm{sim}}$ at the sampling sites. In a second model variant (TU, "tau unknown"), we also include τ among the unknown parameters, while maintaining $\overline{C}^{\mathrm{obs}} = \overline{C}^{\mathrm{sim}}$. A third model variant (ME, "measurement error") is obtained by perturbing $\overline{C}^{\mathrm{sim}}$ by accounting for a probability of non-detection (as in Carraro, Hartikainen, et al. (2018)) and a measurement error. In particular, we calculate $\overline{C}^{\mathrm{obs}}$ as:

$$\overline{C}_i^{\mathrm{obs}} = \begin{cases} 0 & \text{with probability } \exp\left(-\overline{C}_i^{\mathrm{sim}}\right), \\ \exp\left(K_i\right),\ K_i \sim \mathcal{N}\left(\ln \overline{C}_i^{\mathrm{sim}}, 0.5\right) & \text{with probability } 1-\exp\left(-\overline{C}_i^{\mathrm{sim}}\right), \end{cases} \tag{6}$$

Equation (6) states that low concentrations $\overline{C}^{\mathrm{sim}}$ are more likely to result in false negatives (that is, non-detections): for instance, if $\overline{C}_i^{\mathrm{sim}} = 1$, there is a $\exp(-1) \approx 36.7\%$ chance to not detect eDNA at site *i*. Moreover, it assumes that observed concentrations $\overline{C}^{\mathrm{obs}}$ are lognormally distributed around the values $\overline{C}^{\mathrm{sim}}$ calculated in step 2. The choice of the lognormal distribution is justified by the fact that such distribution does not allow false positives (i.e., if $\overline{C}_i^{\mathrm{sim}} = 0$ then it must be $\overline{C}_i^{\mathrm{obs}} = 0$). We are aware that false positives in eDNA detection might arise due to, for example, contamination (Ficetola et al., 2016), but we deem this circumstance beyond the scope of our

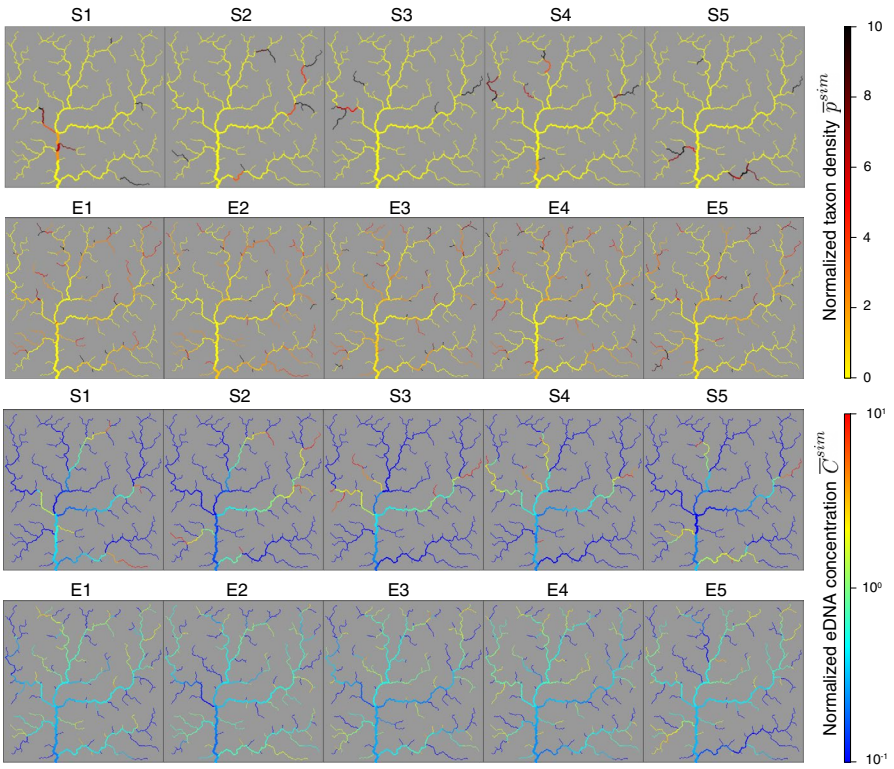

FIGURE 3 Overview of the ten different maps of normalized taxon density $\overline{p}^{\mathrm{sim}}$ and the corresponding normalized eDNA concentrations $\overline{C}^{\mathrm{sim}}$ generated (in step 1 and 2 of Figure 2, respectively). In maps of$\overline{p}^{\mathrm{sim}}$, the apparent bias toward upstream nodes is due to the fact that downstream nodes are characterized by larger source area A_s (in turn, caused by larger river width in the downstream direction). Therefore, the corresponding taxon density $\overline{p}_j^{\mathrm{sim}}$ calculated with Equation (5) tends to be lower for a downstream node as compared to the value a headwater picked as hotspot (note the $A_{S,j}$ at the denominator)

work. Moreover, in model variant ME, τ is assumed to be unknown in the fitting process. Finally, to assess the robustness of our analysis with respect to our assumptions on decay time and hydrological conditions, we perform additional simulations where such assumptions were altered. Full details are provided in the Appendix S1.

2.4.5 | Model fitting

We fit the models by assuming independent and identically distributed Gaussian errors between modeled ($\overline{C}^{\mathrm{mod}}$) and observed ($\overline{C}^{\mathrm{obs}}$) concentrations. Evidence suggests that eDNA concentration in the field might follow a lognormal distribution (Fukaya et al., 2020; Jo et al., 2017); however, we opted for a normal distribution because it is also directly applicable to null eDNA concentrations, which is not the case for the lognormal distribution. For all three model variants, the so-obtained log-likelihood is maximized by means of the *optimParallel* R-package (Gerber & Furrer, 2019). Due to the large number of parameters (see next paragraph), we opted to fix the standard deviation of the Gaussian errors between $\overline{C}^{\mathrm{mod}}$ and $\overline{C}^{\mathrm{obs}}$ to 2, in order to facilitate model calibration and comparison of results.

For each model, the number of unknowns is equal to 200 (number of nodes where $\overline{p}^{\mathrm{mod}}$ is to be calculated) plus 1 (parameter τ, only for model variants TU and ME), while the number of observations is equal to 20, 50 or 100, depending on the sampling intensity. The fact that the number of unknowns is higher than the number of observation is likely to lead to equifinality (sensu Beven & Freer, 2001, that is, different combination of parameters may be equally able to reproduce the observed behavior of a system). Note, however, that this is not a drawback of our approach: indeed, models with a higher degree of indetermination (i.e., less observations, as with a sampling intensity of 10%) will tend to be more affected by equifinality than models with a higher number of observations (e.g., with a sampling intensity of 50%), and therefore will tend to perform worse in terms of prediction skill (see next section). Observing how much the predictive power of a model worsens if a lower number of sites is chosen, and assessing how much this depends on sites' positioning and/or the underlying taxon distribution are aspects that we aim to investigate with our approach.

All $\overline{p}^{\mathrm{mod}}$ values are constrained between 0 and 250; for models TU and ME, τ is constrained between 1 and 251 hr. By setting a lower bound of 1 hr for τ, we forced the calibration algorithm to consider downstream transportation of eDNA when estimating the $\overline{p}^{\mathrm{mod}}$ parameters. Failing to do so would often lead to model estimates of τ close to 0 and, as a result, totally arbitrary values of $\overline{p}^{\mathrm{mod}}$ in the unsampled sites, because they would have no impact in the log-likelihood (i.e., all upstream eDNA contribution would be totally degraded before reaching any sampling site).

2.4.6 | Assessment of prediction skill

The last step of the computer simulation consists in comparing the estimated map of taxon distribution ($\overline{p}^{\mathrm{mod}}$) with the original pattern ($\overline{p}^{\mathrm{sim}}$) generated in step 1. To do so, we formulate two different criteria: The first one focuses on predictions of presence and absence at the various river reaches, while the second compares values of taxon density.

The first criterion (termed *PA*) expresses the fraction of river reaches where presence or absence was correctly predicted. Since values of $\overline{p}^{\mathrm{mod}}$ are always larger than zero due to numerical approximations of the model fitting process, we need to impose threshold values in order to convert a map of relative taxon density into a map of occurrences. In particular, we attribute the threshold $\overline{p}_i^{\mathrm{sim}} \le 1/4$ for absence and $\overline{p}_i^{\mathrm{sim}} \ge 1/5$ for presence; the small overlap allows, for example, $\overline{p}_i^{\mathrm{mod}} = 0.22$ to be a correct estimate of $\overline{p}_i^{\mathrm{sim}} = 0.21$. *PA* reads then:

$$\mathrm{PA} = \frac{1}{N}\sum_{i=1}^{N}\left\{\left[\left(\overline{p}_i^{\mathrm{mod}} \le \frac{1}{4}\right) \wedge \left(\overline{p}_i^{\mathrm{sim}} \le \frac{1}{4}\right)\right] \vee \left[\left(\overline{p}_i^{\mathrm{mod}} \ge \frac{1}{5}\right) \wedge \left(\overline{p}_i^{\mathrm{sim}} \ge \frac{1}{5}\right)\right]\right\} \tag{7}$$

where $\{X\}$ is to be intended as an indicator function, namely equal to 1 if event X is true, and null otherwise.

The second criterion (termed *D*) expresses the fraction of river reaches where the modeled taxon density $\overline{p}^{\mathrm{mod}}$ is deemed a good estimate of $\overline{p}^{\mathrm{sim}}$:

$$D = \frac{1}{N}\sum_{i=1}^{N}\left\{\left[\left(\overline{p}_i^{\mathrm{mod}} \le \frac{1}{4}\right) \wedge \left(\overline{p}_i^{\mathrm{sim}} \le \frac{1}{4}\right)\right] \vee \left[\left(\overline{p}_i^{\mathrm{mod}} \ge \frac{3}{4}\overline{p}_i^{\mathrm{sim}}\right) \wedge \left(\overline{p}_i^{\mathrm{mod}} \le \frac{4}{3}\overline{p}_i^{\mathrm{sim}}\right)\right]\right\}. \tag{8}$$

In other words, according to this criterion, $\overline{p}_i^{\mathrm{sim}}$ is correctly predicted if the corresponding $\overline{p}_i^{\mathrm{mod}}$ is between 75% and 133% of its value; moreover, if $\overline{p}_i^{\mathrm{sim}}$ is lower than or equal to 1/4 (hence presumably indicating absence of the taxon in that node), then it must also be $\overline{p}_i^{\mathrm{mod}} \le 1/4$. A graphical representation of the two criteria is provided in Figure S3. Finally, to test the robustness of our analysis with respect to the values of the thresholds used to define *PA* and *D*, we also calculate alternative prediction skill criteria based on modified threshold values. All details are reported in the Appendix S1.

3 | RESULTS

3.1 | Analysis of eDNA concentration patterns across a river network

Environmental DNA concentration patterns across the OCN as a function of different taxon distributions and decay time values are presented in Figure 4. Remarkably, when the normalized taxon distribution $\overline{p}$ is uniform and no eDNA decay occurs ($\tau \to \infty$), the resulting eDNA concentration pattern (Figure 4a) is not uniform but rather increases downstream, and reaches its maximum value $\overline{C} = 1$ at the outlet (as expected from Equation (4)). This result can intuitively be explained by the fact that a portion of habitat of unit stream length (in our case, a pixel) located downstream is characterized by a larger width than an analogous portion of habitat located upstream.

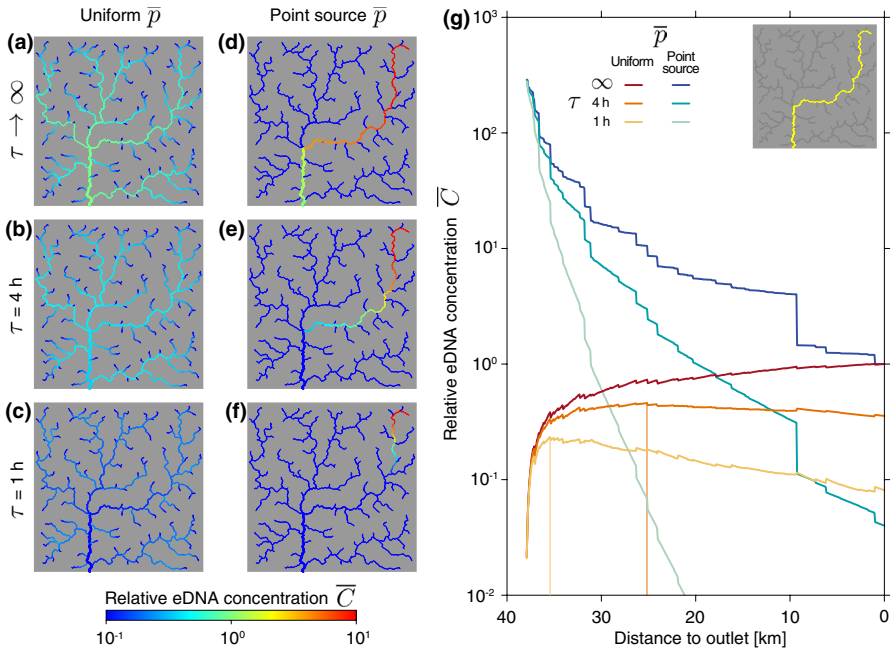

FIGURE 4 Effect of taxon distribution and eDNA decay processes on spatial patterns of eDNA concentration. (a–f) Maps of relative eDNA concentration $\overline{C}$ for uniform (panels a–c) and point source (panels d–f) distributions of normalized taxon density $\overline{p}$ and no decay dynamics (panels a, d), $\tau = 4$ hr (panels b, e), $\tau = 1$ hr (panels c, f). In the point source scenario, the taxon is concentrated in the pixel representing the headwater of the main river stem (i.e., the farthest point from the outlet). (g) Profiles of $\overline{C}$ along the main river stem (depicted in yellow in the inset, and corresponding to the longest path from a source to the outlet) for the six maps displayed in panels (a–f). Vertical colored lines identify positions of maxima of $\overline{C}$ for profiles corresponding to maps on panels b and c

Hence, at the downstream portion of habitat, uniform taxon density implies higher abundance, and in turn, higher amount of eDNA shed. As a result, in this scenario eDNA concentration increases in the downstream direction. A more formal explanation is provided in the Appendix S1.

The above-described pattern of increasing concentration in the downstream direction can be altered in the presence of eDNA decay. When $\overline{p}$ is uniform, the decay process induces a decreasing pattern of $\overline{C}$ in the downstream direction in the region that is closer to the outlet, while, in the upstream reaches, $\overline{C}$ increases downstream for the aforementioned reasons (Figure 4b,c). As a result, the profile of concentration along the main stem is unimodal, and the location where $\overline{C}$ is maximized is controlled by the value of decay time (being shifted downstream for increasing values of τ, see vertical colored lines in Figure 4g).

When $\overline{p}$ is concentrated in a single source and $\tau \to \infty$ (Figure 4d), eDNA concentration decreases downstream as a result of dilution because of water coming from "clean" tributaries. The concentration profile along the main stem (Figure 4g) is characterized by a number of vertical steps, which correspond to the confluences with the main tributaries. The inclusion of eDNA decay dynamics (Figure 4e,f) enhances the decreasing trend of $\overline{C}$, such that concentration values at the outlet are considerably lower than the corresponding values obtained with equal values of τ but uniform distribution for $\overline{p}$.

3.2 | Effect of sampling strategy

Aggregated results on the prediction skill expressed in terms of the presence/absence (*PA*) criterion (Equation (7)) are shown in Figure 5. As expected, higher sampling intensity leads to better prediction skill, all other factors being equal. When the taxon is concentrated in few hotspots across the river network (S distributions) and only 10% of the sites are sampled (Figure 5a), the most reliable strategy is to preferentially sample the downstream sites (positioning U0), and the performance of the various strategies decreases with increasing percentage of sites sampled in the upstream region. Notably, with the aforementioned settings (i.e., S distribution, few sampling sites), this result holds regardless of the model variant; furthermore, in most of the simulations (and especially for upstream-biased strategies), the resulting *PA* score is not higher than the value of 0.5 that would be expected for a random choice of $\overline{p}^{\text{mod}}$. If the fraction of sampling sites increases (Figure 5b,c), sampling designs tend to perform better than random. Moreover, the trend of increasing performance with increasing percentage of sampling sites in the downstream region holds only if perfect knowledge of the decay time and no uncertainty in eDNA measurements are assumed (model variant TF); for the other model variants, more balanced strategies (U20 or U50) are to be preferred (Figure 5b), or even strategies that preferentially include upstream sites (U80) when the fraction of sampled sites is increased to 50% (Figure 5c, model ME).

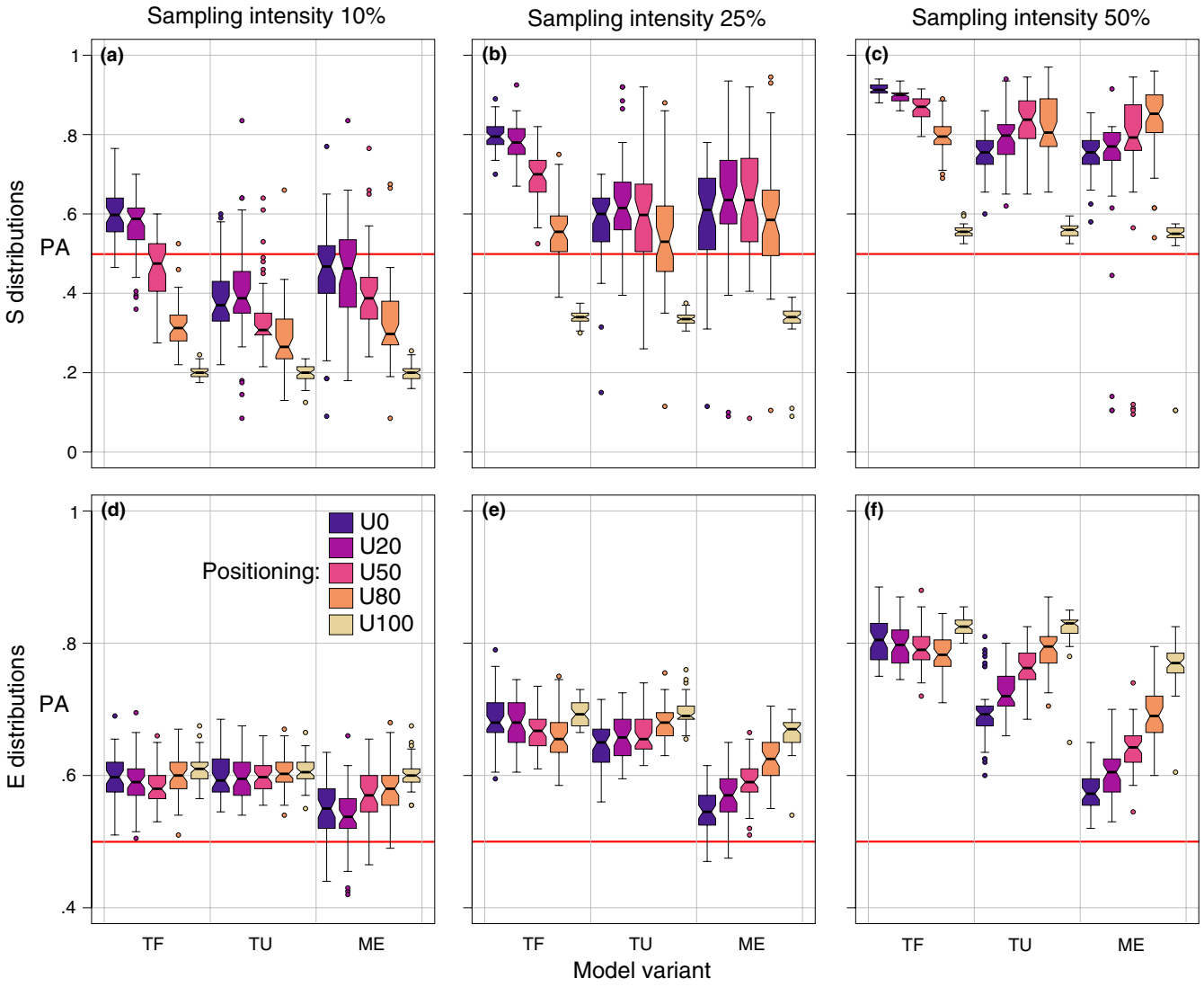

FIGURE 5 Boxplots of values of the presence/absence (*PA*) criterion. Each boxplot is representative of 50 model runs (5 taxon distribution realizations times 10 sampling strategy realizations). Top (panels a, b, c) and bottom (panels d, e, f) rows refer to taxon distribution types S (scattered) and E (even), respectively. Columns refer to different sampling intensities. Red horizontal lines identify the value $PA = 0.5$, corresponding to the expected score of a random presence/absence predictor. Model variants are TF ("tau fixed"), TU ("tau unknown"), ME ("measurement error")

When instead the taxon is more evenly distributed across the catchment (E distributions - Figure 5d–f), the prediction skill is generally less sensitive to the sampling intensity and strategy: Indeed, *PA* is above 0.4 with as few as 20 sampling sites (Figure 5d), for any strategy and model variant. Increasing sampling intensity to 50% only leads to mild improvements in prediction skill: *PA* is seldom (30.3% of the simulations) greater than 0.8 (Figure 5f), while this was more often the case (47.7% of the simulations) for the S distributions (Figure 5c). In general, for taxon distributions of the E type, the most convenient sampling strategy is to preferentially sample in the upstream region (U100), especially when the decay time is unknown and observed eDNA concentrations are affected by measurement error (model ME). The reason for such finding is that patterns of $\overline{C}^{obs}$ of type E are rather noisy, which makes it difficult for the eDITH model to disentangle the various contributions to the eDNA signal; preferentially sampling the upstream sites hence leads to improved predictions at the upstream reaches, since these signals are representative of few (or single) sources and thus easier to interpret.

Figure S4 shows prediction skill of the eDITH model expressed in terms of the density (*D*) criterion (Equation (8)). Results are generally very similar to those discussed for the *PA* criterion. The main difference is that, while values of *D* are only slightly lower than the corresponding values of *PA* for taxon distributions of the S type (compare the top row of Figure S4 with the top row of Figure 5), the same is not true for taxon distributions of the E type: In this case, the fraction of sites where taxon density is correctly predicted is almost never (0.004% of the simulations) above 60% (Figure S4d–f), while the fraction of sites where the presence/absence status is correctly predicted is often (71.9% of the simulations) above 60% (Figure 5).

Remarkably, model variant TF generally performs better than other variants, all other factors and prediction skill criteria being equal. Instead, results obtained for model variant ME are not consistently worse than those obtained for variant TU (all other factors and prediction skill criteria being equal), despite the fact that, in the former model variant, observed concentrations $\overline{C}^{obs}$ are affected by false negatives and measurement errors. In particular, when the taxon distribution is characterized by few hotspots, model variant ME performs similarly to (and, at times, better than) model TU (top rows of Figure 5 and Figure S4). Conversely, considering false negatives and measurement errors worsens the prediction skill of the eDITH model when the taxon is more evenly distributed (bottom rows of Figure 5 and Figure S4). To explain such finding, it has to be noted that, in the taxon distributions of type E, eDNA concentrations $\overline{C}^{sim}$ are often rather low (say, between 0.1 and 1, see Figure 3) and therefore possibly interpreted as false negatives, according to Equation (6). Instead, in the S distributions, patterns of $\overline{C}^{sim}$ are characterized by few locations where the concentration is very high and unlikely to lead to a non-detection, resulting in observed values $\overline{C}^{obs}$ that are less perturbed. As a result, when τ is not known but there is a strong observed eDNA signal, the presence of a measurement error on $\overline{C}^{obs}$ does not impact the estimates on taxon distribution performed by the eDITH model: Indeed, the resulting $\overline{p}^{mod}$ pattern will anyways resemble the real taxon distribution (at least to the same degree as if eDNA concentrations could be measured without error—see Figures S5 and S6), with the possible drawback that the estimate of τ might be less accurate. As shown in Figure 6 in fact, values of the decay time estimated by the model variant ME are farther from the correct value $\tau = 4$ hr with respect to the TU model, and tend to coincide with the lower bound $\tau = 1$ hr imposed in the model fitting process, indicating failure in the determination of the value for such parameter.

As expected, an increase in sampling intensity leads to estimates of the decay time τ that are closer to the correct value $\tau = 4$ hr, all other factors being equal (Figure 6). In general, sampling strategies with preferential sampling at the downstream sites tend to lead to an underestimation of the decay time, while the opposite is true for sampling strategies with higher fraction of sites chosen among the upstream reaches (Figure 6). As a result, more balanced (e.g., U50) strategies might be more likely to accurately estimate the decay time dynamics. The fact that upstream-biased strategies tend to

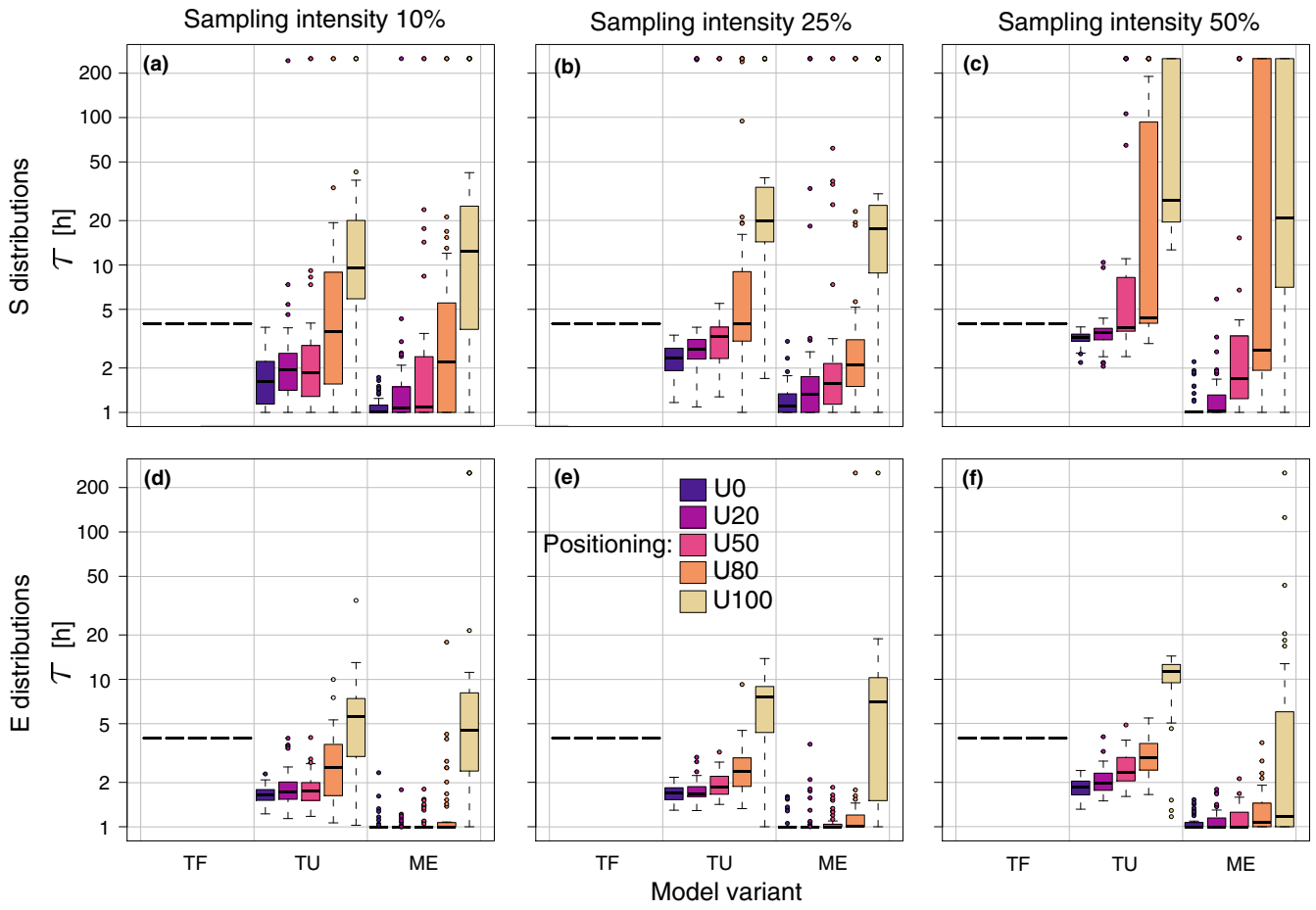

FIGURE 6 Boxplots of decay time values (in logarithmic scale) estimated by the model fitting procedure (step 4 of Figure 2). Each boxplot is representative of 50 model runs (5 taxon distribution realizations times 10 sampling strategy realizations). Top (panels a, b, c) and bottom (panels d, e, f) rows refer to taxon distribution types S (scattered) and E (even), respectively. Model variants are TF ("tau fixed"), TU ("tau unknown"), ME ("measurement error")

overestimate decay times (and, consequently, underestimate decay velocity) is explained by considering that these sampling schemes are characterized by a reduced degree of nestedness, namely the fraction of sampling sites that are connected by flow is low (details are provided in the Appendix S1). Indeed, in order to correctly assess decay dynamics, it is crucial to sample eDNA multiple times along the flow direction; if this was not the case, measurements from a single sample site that is not accompanied by other sampling sites upstream would make it impossible to disentangle the relative contributions of shedding (proportional to taxon density) and decay dynamics in the eDNA signal collected.

4 | DISCUSSION

Inferences of biodiversity based on riverine DNA data that go beyond the mere presence/absence status of organisms at the catchment level (i.e., gamma diversity only) need to consider hydromorphological processes that control advection and decay of eDNA in stream water. In this work, we have exploited a hydrology-based eDNA transport model applied to a virtual—yet realistic—river network in order to analyze patterns of eDNA concentration across a river network and assess optimal strategies for eDNA sampling. Indeed, we found that spatial patterns of eDNA concentration are shaped by the scaling character of dendritic river networks: In particular, because of the power-law scaling of hydrological variables (chiefly river width), even a uniform taxon distribution does not lead to a uniform pattern of eDNA concentration, even if decay dynamics are neglected.

Our most important result is that selection of an optimal sampling strategy requires basic knowledge on the expected taxon distribution. When a taxon is expected to be concentrated in a few hotspots (e.g., as in the case of endangered and often only locally occurring organisms, such as the freshwater pearl mussel (*Margaritifera margaritifera*)) and sampling can be performed only at few sites due to time or budget constraints, it is advisable to preferentially sample the downstream locations; if, at a later stage, further sampling sites can be added, these should better be located in the upstream portion of the catchment. In such a case, the prediction skill of the eDITH model is quite sensitive to the number of sampling sites, and the fraction of sites where taxon density is correctly predicted does not change substantially with respect to the value related to correct presence/absence prediction. Conversely, when the taxon is distributed in a more uniform way across the catchment (e.g., as known for many widely distributed and common species, such as the freshwater amphipod *Gammarus fossarum* or brown trout (*Salmo trutta*)), both number and positioning of sampling sites have a limited effect in improving the prediction skill of the model, and thus also the overall detection and resolution of biodiversity patterns of organisms across the catchment. Indeed, in such a case, values of observed eDNA concentration will tend not to differ much across sites, which complicates the localization of the main sources where eDNA is shed. However, we found that a preferential sampling of upstream sites might give slightly better overall predictions. Actually, in this case the improvement of prediction skill given by this strategy is limited to the upstream parts of the catchment, because the eDNA measurements collected therein would be representative of a lower number of sources and hence more easily interpretable by the eDITH model. In general, when the taxon is rather uniformly distributed, the presence/absence status can be fairly well predicted even with a limited number of sampling sites, while estimates of taxon density are much poorer than in the case when the taxon is located in few hotspots. Importantly, our additional simulations (see Appendix S1) showed that the aforementioned best-practice strategies hold irrespective of assumptions on decay time, hydrological conditions, and threshold values used to define the prediction skill criteria.

As expected, we observed that knowing the value of the decay time τ generally leads to improved prediction skill. Recently, research interest in the assessment of decay rates of eDNA collected from freshwater has expanded considerably (Eichmiller et al., 2016; Lance et al., 2017; Sassoubre et al., 2016; Seymour et al., 2018; Tsuji et al., 2017). Such insights are of great help in improving the reliability of predictions of taxon distribution performed by the eDITH model, at least by allowing the determination of a narrow feasible range for this parameter. If instead τ is unknown, estimates of the taxon distribution operated by eDITH can still be fairly reliable, although the estimate of τ given by the model can be inaccurate. Measurement errors, which include all possible sources of uncertainties arising from the eDNA collection and sequencing processes, can indeed perturb the observed values of eDNA concentration, but they do not hinder the possibility to correctly estimate the taxon distribution, especially if the taxon is concentrated in a limited number of hotspots.

In order to perform a distinction between the various sampling strategies, we operated a partitioning of the reaches constituting the river network into upstream and downstream sites based on the distribution of drainage area values across the sites. It has to be noted that, owing to the criterion adopted, those marked as "downstream" sites do not only correspond to locations along the main stem and close to the river outlet, but also to sites that are rather distant from it (see Figure 1). Moreover, the so-obtained OCN has a drainage density (i.e., the ratio between total length of the river network and drainage area) of 0.7 km-1, which is representative of a very arid catchment (typical values of drainage density range from 2 to 20 km^{-1}, with higher values corresponding to intermediate values of annual precipitation (Moglen, Eltahir, & Bras, 1998)). We refrained from using an OCN with higher drainage density because this would have implied increasing the dimensionality of the problem, which would have hindered the convergence of the calibration algorithm, and likely jeopardized the prediction skill of the model. This implies that the headwater streams shown in Figure 1 (marked with red dots, and corresponding to the “upstream” sites of the computer simulations) are not likely to correspond to reaches of Strahler stream order equal to 1 of a real catchment of the same size, but rather to larger reaches, with Strahler order values of at least 2. Consequently, sites here marked as “downstream” are (roughly) representative of real stream reaches with Strahler order greater than 2.

Importantly, to perform the computer simulations, we partitioned the river network at the reach scale, whereby we considered reaches as river stretches not containing confluences and not longer than 2.5 km. By doing so, we implicitly assumed that sampling more than once along a single river reach is sub-optimal, because this would lead to measurements whose information content is overlapping. In general, we suggest to choose sampling sites such that their pairwise along-stream distance is of at least a couple of kilometers (for instance, in this application we fixed the maximum reach length equal to 2.5 km), so that they are representative of subcatchments that are rather distinguished. However, in the presence of high stochasticity (and/or high likelihood of non-detection) of measured eDNA concentrations within a single site, it might be relevant to perform multiple sampling at the same site. Potentially, the number of samples taken at a site might change with the site's position across the river network (e.g., more samples per site taken at the downstream locations, as suggested by Bylemans et al., 2018). A possible development of our modeling work could actually test this hypothesis. Collecting more samples at fixed downstream locations would also be beneficial because, due to a dilution effect, eDNA concentrations at the downstream sites are likely not high even in the presence of a local taxon hotspot (see Figure 3), and hence more prone to result in non-detections. This is especially important in the context of many metabarcoding studies setting thresholds of read numbers below which the signal is no longer accepted as a true positive (Deiner et al., 2017; Mächler, Walser, & Altermatt, 2020). In this perspective, collecting larger water volumes at the downstream sites is likely to help minimize the risk of non-detection.

In this study, for the sake of simplicity, we focused on localization of a single taxon within a river basin. However, the eDITH model herein adopted can also be applied repeatedly with eDNA data for different taxa collected at the same sites (also in the form of metabarcoding data, i.e., read numbers) in order to estimate spatial patterns of biodiversity, provided that an appropriate statistical relationship between read numbers and the underlying eDNA concentration is adopted (Carraro, Mächler, et al., 2020). Moreover, eDITH can be theoretically used with any taxonomic group, given that no specific assumption on the eDNA production rate p is made, its value being directly inferred from the eDNA concentration data. In particular, its application on motile taxa (e.g., fish or crustaceans) is guaranteed because the scale distance of mobility of most organisms is typically much shorter than that of hydrological transport in rivers (Carraro, Mächler, et al., 2020). Hence, the findings of the present study could potentially be generalized to the issue of determining the optimal sampling strategy within a river network in order to maximize information on the spatial distribution of biodiversity.

In summary, our study revealed potential strategies to optimize the design of eDNA sampling campaigns in river networks. Notably, the insights gained by our modeling approach need be paired by biological and empirical knowledge on the investigated taxon: In fact, the choice of the optimal sampling design relies on preliminary knowledge on the expected distribution of the taxon, and on whether or not estimates of eDNA decay rates in the environment are available. Coupling modeling and empirical evidence on eDNA transport and decay processes is thereby crucial in order to fully exploit the power of eDNA to monitor freshwater biodiversity.

ACKNOWLEDGMENTS

FA acknowledges support from the Swiss National Science Foundation grants No. PP00P3_179089 and 31003A_173074 as well as from the University of Zurich Research Priority Programme "URPP Global Change and Biodiversity." We thank Jeanine Brantschen and Rosetta C. Blackman for valuable comments on the manuscript.

CONFLICT OF INTEREST

None declared.

AUTHOR CONTRIBUTIONS

LC and FA developed the idea, LC conceptualized the work and wrote the first draft of the manuscript. LC and JBS analyzed the data. All authors contributed to the final manuscript version.

DATA AVAILABILITY STATEMENT

All data and codes necessary to reproduce the results of the manuscript are available at https://doi.org/10.5281/zenodo.4009202.

ORCID

Luca Carraro https://orcid.org/0000-0002-3933-1144
Florian Altermatt https://orcid.org/0000-0002-4831-6958

REFERENCES

Alberdi, A., Aizpurua, O., Gilbert, M. T. P., & Bohmann, K. (2017). Scrutinizing key steps for reliable metabarcoding of environmental samples. *Methods in Ecology and Evolution*, *9*(1), 134–147. https://doi.org/10.1111/2041-210x.12849

Altermatt, F. (2013). Diversity in riverine metacommunities: A network perspective. *Aquatic Ecology*, *47*(3), 365–377. https://doi.org/10.1007/s10452-013-9450-3

Altermatt, F., Little, C. J., Mächler, E., Wang, S., Zhang, X., & Blackman, R. C. (2020). Uncovering the complete biodiversity structure in spatial networks: The example of riverine systems. *Oikos*, *129*(5), 607–618. https://doi.org/10.1111/oik.06806

Alther, R., & Altermatt, F. (2018). Fluvial network topology shapes communities of native and non-native amphipods. *Ecosphere*, *9*(2), e02102. https://doi.org/10.1002/ecs2.2102

Andruszkiewicz, E. A., Koseff, J. R., Fringer, O. B., Ouellette, N. T., Lowe, A. B., Edwards, C. A., & Boehm, A. B. (2019). Modeling environmental DNA transport in the coastal ocean using lagrangian particle tracking. *Frontiers in Marine Science*, *6*, 477. https://doi.org/10.3389/fmars.2019.00477

Barnes, M. A., & Turner, C. R. (2015). The ecology of environmental DNA and implications for conservation genetics. *Conservation Genetics*, *17*(1), 1–17. https://doi.org/10.1007/s10592-015-0775-4

Barnes, M. A., Turner, C. R., Jerde, C. L., Renshaw, M. A., Chadderton, W. L., & Lodge, D. M. (2014). Environmental conditions influence eDNA persistence in aquatic systems. *Environmental Science & Technology*, *48*(3), 1819–1827. https://doi.org/10.1021/es404734p

Beng, K. C., & Corlett, R. T. (2020). Applications of environmental DNA (eDNA) in ecology and conservation: Opportunities, challenges and prospects. *Biodiversity and Conservation*, *29*, 2089–2121. https://doi.org/10.1007/s10531-020-01980-0

Besemer, K., Singer, G., Quince, C., Bertuzzo, E., Sloan, W., & Battin, T. J. (2013). Headwaters are critical reservoirs of microbial diversity for fluvial networks. *Proceedings of the Royal Society B: Biological Sciences*, *280*(1771), 20131760. https://doi.org/10.1098/rspb.2013.1760

Beven, K., & Freer, J. (2001). Equifinality, data assimilation, and uncertainty estimation in mechanistic modelling of complex environmental systems using the GLUE methodology. *Journal of Hydrology*, *249*(1–4), 11–29. https://doi.org/10.1016/S0022-1694(01)00421-8

Bohmann, K., Evans, A., Gilbert, M. T. P., Carvalho, G. R., Creer, S., Knapp, M., … de Bruyn, M. (2014). Environmental DNA for wildlife biology and biodiversity monitoring. *Trends in Ecology and Evolution*, *29*(6), 358–367. https://doi.org/10.1016/j.tree.2014.04.003

Bylemans, J., Gleeson, D. M., Lintermans, M., Hardy, C. M., Beitzel, M., Gilligan, D. M., & Furlan, E. M. (2018). Monitoring Riverine Fish Communities through eDNA metabarcoding: Determining optimal sampling strategies along an altitudinal and biodiversity gradient. *Metabarcoding and Metagenomics*, *2*, e30457. https://doi.org/10.3897/mbmg.2.30457

Calderón-Sanou, I., Münkemüller, T., Boyer, F., Zinger, L., & Thuiller, W. (2019). From environmental DNA sequences to ecological conclusions: How strong is the influence of methodological choices? *Journal of Biogeography*, *47*, 193–206. https://doi.org/10.1111/jbi.13681

Carraro, L., Altermatt, F., Fronhofer, E. A., Furrer, R., Gounand, I., Rinaldo, A., & Bertuzzo, E. (2020). *OCNet: Optimal Channel Networks*. *R Package Version 0.3.1*.

Carraro, L., Bertuzzo, E., Fronhofer, E. A., Furrer, R., Gounand, I., Rinaldo, A., & Altermatt, F. (2020). Generation and application of river network analogues for use in ecology and evolution. *Ecology and Evolution*, *10*(14), 7537–7550. https://doi.org/10.1002/ece3.6479

Carraro, L., Bertuzzo, E., Mari, L., Fontes, I., Hartikainen, H., Strepparava, N., … Rinaldo, A. (2017). Integrated field, laboratory, and theoretical study of PKD spread in a Swiss Prealpine river. *Proceedings of the National Academy of Sciences of the United States of America*, *114*(45), 11992–11997. https://doi.org/10.1073/pnas.1713691114

Carraro, L., Hartikainen, H., Jokela, J., Bertuzzo, E., & Rinaldo, A. (2018). Estimating species distribution and abundance in river networks using environmental DNA. *Proceedings of the National Academy of Sciences of the United States of America*, *115*(46), 11724–11729. https://doi.org/10.1073/pnas.1813843115

Carraro, L., Mächler, E., Wüthrich, R., & Altermatt, F. (2020). Environmental DNA allows upscaling spatial patterns of biodiversity in freshwater ecosystems. *Nature Communications*, *11*(1), 3585. https://doi.org/10.1038/s41467-020-17337-8

Carraro, L., Mari, L., Gatto, M., Rinaldo, A., & Bertuzzo, E. (2018). Spread of proliferative kidney disease in fish along stream networks: A spatial metacommunity framework. *Freshwater Biology*, *63*(1), 114–127. https://doi.org/10.1111/fwb.12939

Darwall, W., Bremerich, V., De Wever, A., Dell, A. I., Freyhof, J., Gessner, M. O., … Weyl, O. (2018). The alliance for freshwater life: A global call to unite efforts for freshwater biodiversity science and conservation. *Aquatic Conservation: Marine and Freshwater Ecosystems*, *28*(4), 1015–1022. https://doi.org/10.1002/aqc.2958

Deiner, K., & Altermatt, F. (2014). Transport distance of invertebrate environmental DNA in a natural river. *PLoS One*, *9*(2), e88786. https://doi.org/10.1371/journal.pone.0088786

Deiner, K., Bik, H. M., Mächler, E., Seymour, M., Lacoursière-Roussel, A., Altermatt, F., … Bernatchez, L. (2017). Environmental DNA metabarcoding: Transforming how we survey animal and plant communities. *Molecular Ecology*, *26*(21), 5872–5895. https://doi.org/10.1111/mec.14350

Deiner, K., Fronhofer, E. A., Mächler, E., Walser, J.-C., & Altermatt, F. (2016). Environmental DNA reveals that rivers are conveyer belts of biodiversity information. *Nature Communications*, *7*(1), 12544. https://doi.org/10.1038/ncomms12544

Dickie, I. A., Boyer, S., Buckley, H. L., Duncan, R. P., Gardner, P. P., Hogg, I. D., … Weaver, L. (2018). Towards robust and repeatable sampling methods in eDNA-based studies. *Molecular Ecology Resources*, *18*(5), 940–952. https://doi.org/10.1111/1755-0998.12907

Dudgeon, D. (2019). Multiple threats imperil freshwater biodiversity in the Anthropocene. *Current Biology*, *29*(19), R960–R967. https://doi.org/10.1016/j.cub.2019.08.002

Eichmiller, J. J., Best, S. E., & Sorensen, P. W. (2016). Effects of temperature and trophic state on degradation of environmental DNA in lake water. *Environmental Science & Technology*, *50*(4), 1859–1867. https://doi.org/10.1021/acs.est.5b05672

Ficetola, G. F., Miaud, C., Pompanon, F., & Taberlet, P. (2008). Species detection using environmental DNA from water samples. *Biology Letters*, *4*(4), 423–425. https://doi.org/10.1098/rsbl.2008.0118

Ficetola, G. F., Taberlet, P., & Coissac, E. (2016). How to limit false positives in environmental DNA and metabarcoding? *Molecular Ecology Resources*, *16*(3), 604–607. https://doi.org/10.1111/1755-0998.12508

Fukaya, K., Murakami, H., Yoon, S., Minami, K., Osada, Y., Yamamoto, S., … Kondoh, M. (2020). Estimating fish population abundance by integrating quantitative data on environmental DNA and hydrodynamic modeling. *Molecular Ecology*. https://doi.org/10.1111/mec.15530

Garlapati, D., Charankumar, B., Ramu, K., Madeswaran, P., & Ramana Murthy, M. V. (2019). A review on the applications and recent advances in environmental DNA (eDNA) metagenomics. *Reviews in Environmental Science and Biotechnology*, *18*(3), 389–411. https://doi.org/10.1007/s11157-019-09501-4

Gerber, F., & Furrer, R. (2019). optimParallel: An R package providing a parallel version of the L-BFGS-B optimization method. *R Journal*, *11*(1), 352–358. https://doi.org/10.32614/RJ-2019-030

Harrison, J. B., Sunday, J. M., & Rogers, S. M. (2019). Predicting the fate of eDNA in the environment and implications for studying biodiversity. *Proceedings of the Royal Society B: Biological Sciences*, *286*(1915), 20191409. https://doi.org/10.1098/rspb.2019.1409

IPBES (2019). *Global assessment report on biodiversity and ecosystem services of the intergovernmental science-policy platform on biodiversity and ecosystem services*. IPBES Secretariat, Editor.

Jane, S. F., Wilcox, T. M., Mckelvey, K. S., Young, M. K., Schwartz, M. K., Lowe, W. H., … Whiteley, A. R. (2015). Distance, flow and PCR inhibition: eDNA dynamics in two headwater streams. *Molecular Ecology Resources*, *15*(1), 216–227. https://doi.org/10.1111/1755-0998.12285

Jerde, C. L., Mahon, A. R., Chadderton, W. L., & Lodge, D. M. (2011). "Sight-unseen" detection of rare aquatic species using environmental DNA. *Conservation Letters*, *4*(2), 150–157. https://doi.org/10.1111/j.1755-263X.2010.00158.x

Jo, T., Murakami, H., Masuda, R., Sakata, M. K., Yamamoto, S., & Minamoto, T. (2017). Rapid degradation of longer DNA fragments enables the improved estimation of distribution and biomass using environmental DNA. *Molecular Ecology Resources*, *17*(6), e25–e33. https://doi.org/10.1111/1755-0998.12685

Kaelin, K., & Altermatt, F. (2016). Landscape-level predictions of diversity in river networks reveal opposing patterns for different groups of macroinvertebrates. *Aquatic Ecology*, *50*(2), 283–295. https://doi.org/10.1007/s10452-016-9576-1

Kelly, R. P., Port, J. A., Yamahara, K. M., Martone, R. G., Lowell, N., Thomsen, P. F., … Crowder, L. B. (2014). Harnessing DNA to improve environmental management. *Science*, *344*(6191), 1455–1456. https://doi.org/10.1126/science.1251156

Lance, R. F., Klymus, K. E., Richter, C. A., Guan, X., Farrington, H. L., Carr, M. R., … Baerwaldt, K. L. (2017). Experimental observations on the decay of environmental DNA from bighead and silver carps. *Management of Biological Invasions*, *8*(3), 343–359. https://doi.org/10.3391/mbi.2017.8.3.08

Leopold, L. B., & Maddock, T. (1953). *The hydraulic geometry of stream channels and some physiographic implications*. Geological Survey Professional Paper 252. Washington, DC: United States Government Printing Office.

Leray, M., Knowlton, N., Ho, S., Nguyen, B. N., & Machida, R. J. (2019). GenBank is a reliable resource for 21st century biodiversity research. *Proceedings of the National Academy of Sciences of the United States of America*, *116*(45), 22651–22656. https://doi.org/10.1073/pnas.1911714116

Little, C. J., Fronhofer, E. A., & Altermatt, F. (2020). Nonlinear effects of intraspecific competition alter landscape-wide scaling up of ecosystem function. *American Naturalist*, *195*(3), 432–444. https://doi.org/10.1086/707018

Mächler, E., Deiner, K., Steinmann, P., & Altermatt, F. (2014). Utility of environmental DNA for monitoring rare and indicator macroinvertebrate species. *Freshwater Science*, *33*(4), 1174–1183. https://doi.org/10.1086/678128

Mächler, E., Little, C. J., Wüthrich, R., Alther, R., Fronhofer, E. A., Gounand, I., … Altermatt, F. (2019). Assessing different components of diversity across a river network using eDNA. *Environmental DNA*, *1*(3), 290–301. https://doi.org/10.1002/edn3.33

Mächler, E., Walser, J.-C., & Altermatt, F. (2020). Decision making and best practices for taxonomy-free eDNA metabarcoding in biomonitoring using hill numbers. Preprint at *BioRxiv*. https://doi.org/10.1101/2020.03.31.017723

Moglen, G. E., Eltahir, E. A. B., & Bras, R. L. (1998). On the sensitivity of drainage density to climate change. *Water Resources Research*, *34*(4), 855–862. https://doi.org/10.1029/97WR02709

Nukazawa, K., Hamasuna, Y., & Suzuki, Y. (2018). Simulating the advection and degradation of the environmental DNA of common Carp along a river. *Environmental Science & Technology*, *52*(18), 10562–10570. https://doi.org/10.1021/acs.est.8b02293

O'Callaghan, J. F., & Mark, D. M. (1984). The extraction of drainage networks from digital elevation data. *Computer Vision, Graphics, and Image Processing*, *28*(3), 323–344. https://doi.org/10.1016/S0734-189X(84)80011-0

Pawlowski, J., Kelly-Quinn, M., Altermatt, F., Apothéloz-Perret-Gentil, L., Beja, P., Boggero, A., … Kahlert, M. (2018). The future of biotic indices in the ecogenomic era: Integrating (E)DNA metabarcoding in biological assessment of aquatic ecosystems. *Science of the Total Environment*, *637–638*(October), 1295–1310. https://doi.org/10.1016/j.scitotenv.2018.05.002

Pont, D., Rocle, M., Valentini, A., Civade, R., Jean, P., Maire, A., … Dejean, T. (2018). Environmental DNA reveals quantitative patterns of fish biodiversity in large rivers despite its downstream transportation. *Scientific Reports*, *8*(1), 10361. https://doi.org/10.1038/s41598-018-28424-8

Reid, A. J., Carlson, A. K., Creed, I. F., Eliason, E. J., Gell, P. A., Johnson, P. T. J., … Cooke, S. J. (2019). Emerging threats and persistent conservation challenges for freshwater biodiversity. *Biological Reviews*, *94*(3), 849–873. https://doi.org/10.1111/brv.12480

Rinaldo, A., Rigon, R., Banavar, J. R., Maritan, A., & Rodriguez-Iturbe, I. (2014). Evolution and selection of river networks: Statics, dynamics, and complexity. *Proceedings of the National Academy of Sciences of the United States of America*, *111*(7), 2417–2424. https://doi.org/10.1073/pnas.1322700111

Rodriguez-Iturbe, I., & Rinaldo, A. (2001). *Fractal river basins. Chance and self-organization*. New York, NY: Cambridge University Press.

Rodriguez-Iturbe, I., Rinaldo, A., Rigon, R., Bras, R. L., Marani, A., & Ijjasz- Vasquez, E. (1992). Energy dissipation, runoff production, and the three-dimensional structure of river basins. *Water Resources Research*, *28*(4), 1095–1103. https://doi.org/10.1029/91WR03034

Sales, N. G., McKenzie, M. B., Drake, J., Harper, L. R., Browett, S. S., Coscia, I., … McDevitt, A. D. (2020). Fishing for mammals: Landscape-level monitoring of terrestrial and semi-aquatic communities using eDNA from riverine systems. *Journal of Applied Ecology*, *57*(4), 707–716. https://doi.org/10.1111/1365-2664.13592

Sansom, B. J., & Sassoubre, L. M. (2017). Environmental DNA (eDNA) shedding and decay rates to model freshwater mussel eDNA transport in a river. *Environmental Science & Technology*, *51*(24), 14244–14253. https://doi.org/10.1021/acs.est.7b05199

Sassoubre, L. M., Yamahara, K. M., Gardner, L. D., Block, B. A., & Boehm, A. B. (2016). Quantification of environmental DNA (eDNA) shedding and decay rates for three marine fish. *Environmental Science and Technology*, *50*(19), 10456–10464. https://doi.org/10.1021/acs.est.6b03114

Schädler, B., & Weingartner, R. (1992). Natural runoff 1961–1980. In M. Spreafico, & R. Weingartner (Eds.), *Hydrological atlas of Switzerland*. Bern, Switzerland: Swiss National Hydrological and Geological Survey.

Sengupta, M. E., Hellström, M., Kariuki, H. C., Olsen, A., Thomsen, P. F., Mejer, H., … Vennervald, B. J. (2019). Environmental DNA for improved detection and environmental surveillance of schistosomiasis. *Proceedings of the National Academy of Sciences of the United States of America*, *116*(18), 8931–8940. https://doi.org/10.1073/pnas.1815046116

Seymour, M., Durance, I., Cosby, B. J., Ransom-Jones, E., Deiner, K., Ormerod, S. J., … Creer, S. (2018). Acidity promotes degradation of multi-species environmental DNA in lotic mesocosms. *Communications Biology*, *1*(1), 4. https://doi.org/10.1038/s42003-017-0005-3

Shogren, A. J., Tank, J. L., Andruszkiewicz, E. A., Olds, B., Jerde, C., & Bolster, D. (2016). Modelling the transport of environmental DNA through a porous substrate using continuous flow-through column experiments. *Journal of the Royal Society Interface*, *13*(119), 20160290. https://doi.org/10.1098/rsif.2016.0290

Shogren, A. J., Tank, J. L., Andruszkiewicz, E., Olds, B., Mahon, A. R., Jerde, C. L., & Bolster, D. (2017). Controls on eDNA movement in streams: Transport, retention, and resuspension. *Scientific Reports*, *7*(1), 5065. https://doi.org/10.1038/s41598-017-05223-1

Shogren, A. J., Tank, J. L., Egan, S. P., August, O., Rosi, E. J., Hanrahan, B. R., … Bolster, D. (2018). Water flow and biofilm cover influence environmental DNA detection in recirculating streams. *Environmental Science and Technology*, *52*(15), 8530–8537. https://doi.org/10.1021/acs.est.8b01822

Strickler, K. M., Fremier, A. K., & Goldberg, C. S. (2015). Quantifying effects of UV-B, temperature, and pH on eDNA degradation in aquatic microcosms. *Biological Conservation*, *183*, 85–92. https://doi.org/10.1016/j.biocon.2014.11.038

Taberlet, P., Coissac, E., Hajibabaei, M., & Riesenberg, L. H. (2012). Environmental DNA. *Molecular Ecology*, *21*(8), 1789–1793. https://doi.org/10.1111/j.1365-294X.2012.05542.x

Thomsen, P. F., Kielgast, J., Iversen, L. L., Wiuf, C., Rasmussen, M., Gilbert, M. T. P., … Willerslev, E. (2012). Monitoring endangered freshwater biodiversity using environmental DNA. *Molecular Ecology*, *21*(11), 2565–2573. https://doi.org/10.1111/j.1365-294X.2011.05418.x

Thomsen, P. F., & Willerslev, E. (2015). Environmental DNA – An emerging tool in conservation for monitoring past and present biodiversity. *Biological Conservation*, *183*, 4–18. https://doi.org/10.1016/j.biocon.2014.11.019

Tsuji, S., Ushio, M., Sakurai, S., Minamoto, T., & Yamanaka, H. (2017). Water temperature-dependent degradation of environmental DNA and its relation to bacterial abundance. *PLoS One*, *12*(4), e0176608. https://doi.org/10.1371/journal.pone.0176608

Vörösmarty, C. J., McIntyre, P. B., Gessner, M. O., Dudgeon, D., Prusevich, A., Green, P., … Davies, P. M. (2010). Global threats to human water security and river biodiversity. *Nature*, *467*(7315), 555–561. https://doi.org/10.1038/nature09440

Wood, Z. T., Erdman, B. F., York, G., Trial, J. G., & Kinnison, M. T. (2020). Experimental assessment of optimal lotic eDNA sampling and assay

multiplexing for a critically endangered fish. *Environmental DNA*. https://doi.org/10.1002/edn3.64

Zurell, D., Berger, U., Cabral, J. S., Jeltsch, F., Meynard, C. N., Münkemüller, T., … Grimm, V. (2010). The virtual ecologist approach: Simulating data and observers. *Oikos*, *119*(4), 622–635. https://doi.org/10.1111/j.1600-0706.2009.18284.x

SUPPORTING INFORMATION

Additional supporting information may be found online in the Supporting Information section.

How to cite this article: Carraro L, Stauffer JB, Altermatt F. How to design optimal eDNA sampling strategies for biomonitoring in river networks. *Environmental DNA*. 2020;00:1–16. https://doi.org/10.1002/edn3.137